ELSEVIER

Cement & Concrete Composites 23 (2001) 267–278

Cement & Concrete Composites

www.elsevier.com/locate/cemconcomp

Image analysis for the automated study of microcracks in concrete

A. Ammouche [a,*], J. Riss [b], D. Breysse [b], J. Marchand [c]

[a] Laboratoire d'Etudes et de Recherches sur les Matériaux (LERM), 23 rue de la Madeleine BP 136, 13631 Arles, France
[b] Centre de Développement des Géosciences Appliquées, Université Bordeaux I, 33405 Talence, France
[c] CRIB- Département de génie civil, Université Laval, Québec, Canada G1K 7P4

Abstract

An image analysis technique for the automated detection and quantification (at the mesoscopic scale) of microcracks in cement-based materials is described. In order to highlight microcracks and other microdefects, the surface of the material is impregnated with a red or a fluorescent dye. Observations of the polished sample are carried out using an optical microscope. The image analysis algorithm developed for the segmentation of the microcracks includes a pretreatment of the color image, an automatic thresholding carried out on the gray level histogram and a treatment of the binary image. The resulting image is then treated using a shape analysis and edge corrections. The characteristics of the crack network are quantitatively determined using classical stereological methods. The technique enables the user to draw maps of the sample crack network over an area of several tens of square centimeters. Results obtained for undamaged and mechanically loaded samples are presented.

Keywords: Concrete; Microcracking; Image analysis; Segmentation; Quantification

1. Introduction

Whatever its origin, the degradation of hydrated cement systems often results in the initiation and the propagation of microcracks. Conventionally, we define microcracks as cracks whose width is about few micrometers (<10 μm). Over the past decade, numerous studies have emphasized the significant influence of microcracks on the mechanical and mass transport properties of concrete [1–4]. Prediction or optimization of the macroscopic properties of a material therefore require the development of a set of reliable tools to quantify its microstructural characteristics.

Over the past 20 years, several techniques have been developed to detect and measure microcracks in cement-based materials [5–14]. The advantages and drawbacks of each of these methods have been critically reviewed in a previous paper [11]. The main difficulties with the quantitative determination of the crack network characteristics of hydrated cement systems can be summarized as follows:

1. Most sample preparation techniques require a predrying treatment, which can alter the original state of the material.
2. Microcrack measurements can vary significantly with magnification and are markedly affected by the degree of resolution of the observation technique. Such a phenomenon originates from the heterogeneous and multi-scale structure of cement-based materials.
3. Manual counting of microcracks is tedious and constitutes a limitation for a systematic analysis. Test results may also be biased by the subjectivity of the operator who often has to convert a complex picture into a binary (yes/no) result.

The determination of the consequences of the degradation on the physical properties (mass transfer, stiffness) of the material obviously requires the quantitative assessment of the crack network characteristics. Measurements often need to be made at different scales.

An image analysis technique that allows the automatic detection of microcracks in concrete is presented in the following sections. The technique was developed to assess the morphological characteristics of microcracks in concrete at the mesoscale. The technique is essentially a three-step process that includes the preparation of the sample, the automatic segmentation of microcracks, and the mathematical treatment of the

* Corresponding author. Fax: +33-4-90-96-25-27.
E-mail address: a.ammouche@lerm.fr (A. Ammouche).

0958-9465/01/$ - see front matter
PII: S0958-9465(00)00054-8

collected data. Results obtained for undamaged and mechanically loaded samples are presented.

2. Microcracks detection using impregnation methods

On the basis of previous works [5,10,11], a simple dye impregnation technique was developed to avoid any bias, which can be induced by the sample preparation. The procedure has been extensively described in a previous paper [11]. In brief, a 15-mm thick disc is cut under water from a laboratory or cored sample, and polished under water with 6-μm diamond paste. The wet polished surface is then impregnated with a red dye [1] solution. The dye in excess is removed by polishing the sample with a 6-μm diamond paste. Finally, progressive polishing with 3- and 1-μm diamond pastes guarantees a good surface quality. Previous experience has shown that observations of the polished surface using an optical microscope at magnification in the range 10–300× is sufficient to highlight the defects of the material including microcracks, paste-aggregate transition zones, porous areas and air bubbles. When applied to ordinary concrete, the technique generates images with a good contrast, which are convenient for a quantitative analysis. The contrast can however be weaker when denser matrices (mixtures of low water/binder ratio or containing supplementary cementing materials) are tested. For instance, the background color (matrice) can be significantly changed with silica fume addition. Furthermore, dense systems are difficult to impregnate. In this case, the red dye can be replaced by a fluorescent dye according to a longer of replacement process. Recent experience has clearly shown that the technique using fluorescent dye is well suited for the observation of microcracks in high performance concrete [15]. According to this technique, the polished sample has to be immersed for four days in an ethanol solution of fluorescent dye. After a slight final polishing, the sample is then ready to be observed using an optical microscope under ultraviolet light.

3. Image analysis algorithms

The various aspects of the algorithms used for the automated image segmentation are described. The various choices made during the development [16,17] of the algorithm (often based on previous practical experience) are described in detail.

All image analysis algorithms were developed under the Visilog 4 environment (Noesis SA, Les Ulis, France). The algorithm allows treating relatively quickly a large number of images, it should be emphasized that in numerous cases, depending on magnification factor between 20× and 80×, more than a thousand images need to be analyzed in order to characterize a single sample of concrete. This requires automatic field by field displacement of the sample, which is done by a motorized stage *x y z* controlled from the microcomputer.

3.1. Automatic segmentation of microcracks

3.1.1. Image acquisition

The procedure first involves the acquisition from the optical microscope of a 256×256-square pixel color image using a tri-CCD camera linked to a personal computer. Each of the three planes *R* (red), *G* (green), and B (blue) results from six individual acquisitions that are averaged in order to reduce any artifacts originating from the electronic noise. Each of these three planes contains 256 possible intensity levels (8 bits: one byte) ranging from 0 for lowest intensity (“black”) to 255 for highest intensity (“white”).

3.1.2. Pre-treatment and segmentation

3.1.2.1. Sample impregnated with red dye (ordinary concrete). Even for ordinary concrete, the contrast between the cracks and the concrete matrix has to be increased prior to the thresholding operation. It should be emphasized that the contrast of an impregnated crack in a microscopic image tends to be influenced by several factors including the porosity of the cement paste, the presence of supplementary cementing materials, the depth of impregnation and the light intensity. The specific intensity levels observed for a given microcrack can also vary with the aperture of the microcrack or other discontinuity. The approach described in this section is convenient for most concrete samples. However, it should be mentioned that the algorithm might need, in some cases, to be adapted to the specific characteristics of the material studied.

In order to perform an optimum image segmentation, it is of fundamental interest to first analyze the intensity level distributions of the three RGB planes, profiles across images and additionally, to measure some particular profiles through microcracks. Figs. 1(a) and (b) show, respectively, typical images of an ordinary concrete impregnated with red dye and their gray level histograms. Some statistical parameters (mean value and standard deviation) are also given. Corresponding red plane and green plane intensity histograms are shown in Figs. 1(c) and (d). It should be noticed that:

- the distributions for the blue and the green planes are very similar (Fig. 1(b)),
- it is seen that the histograms for the red planes show similar shapes to those the blue planes (Fig. 1(b)) but

[1] Commercial name: ‘IRGACET’.

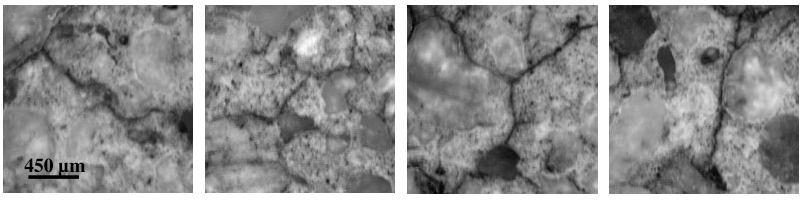

Image 1 Image 2 Image 3 Image 4

(a) color images (40X) - ordinary concrete

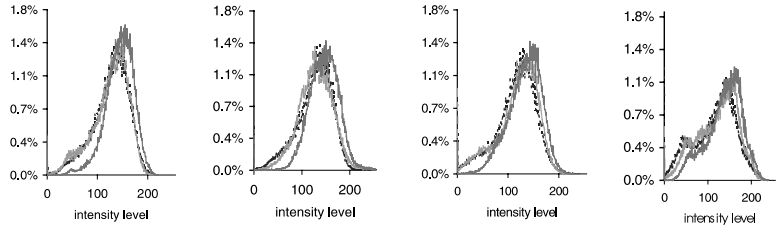

Image 1 Image 2 Image 3 Image 4

	R	G	B		R	G	B		R	G	B		R	G	B
m	143.3	125.0	126.0	m	145.9	128.3	121.9	m	132.5	118.3	114.8	m	137.5	122.0	114.9
σ	29.4	37.1	36.5	σ	31.4	35.9	38.2	σ	33.4	40.8	40.2	σ	41.3	46.4	48.8

(b) Gray level distributions (histograms)

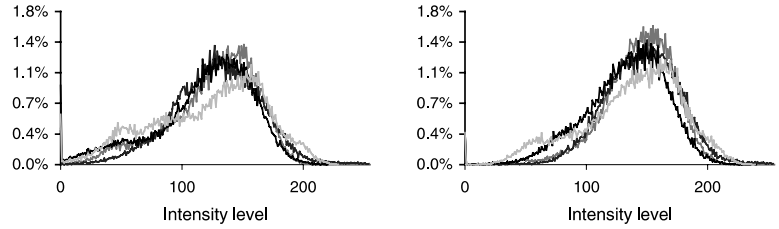

(c) Gray level distributions for the red planes (Images 1, 2, 3, 4)

(d) Gray level distributions for the green planes (Images 1, 2, 3, 4)

Fig. 1. Color images of ordinary concrete and gray level distribution analysis.

they are shifted to the right; mean values are higher for the red planes than for the blue one (differences are approximately 15–20 gray levels),

- all the distributions are more or less bimodal depending on the relative amounts of particles with low intensity level (the highest peak with an intensity level higher than 120, the lowest with an intensity level about 50),
- the gray level distributions for the red and green planes respectively are well superimposed from one image to the other (Figs. 1(c) and (d)).

Figs. 2(a) and (b) show some profiles (intensity level $-y$ axis versus position $-x$ axis) measured through microcracks. It should be noticed that the blue and green profiles present low intensity levels and are similar through the microcracks, while red profiles show higher intensity levels. As a consequence, the difference between the levels of the red and green (or blue) planes is highest through microcracks. However, the same observation can more or less be made about other microdefects (porous zones and air bubbles). Thus, the following arithmetical operation that subtracts the green plane from the red one can be performed to highlight all the impregnated microdefects (microcracks and voids):

$$O(x,y) = \max \begin{cases} R(x,y) - G(x,y), \\ 0. \end{cases} \quad (1)$$

In Eq. (1), $O(x,y)$ stands for the intensity level of the pixel of coordinates (x,y) in the output image. $R(x,y)$ and $G(x,y)$ are the levels of the pixel in the red and green planes, respectively. Fig. 2(c) presents the resulting images. Microcracks are obviously whiter (with higher intensity) than the background and the white pixels are less numerous. The classical thresholding method based on the maximization of the entropy (two classes) of the gray level distribution was found to yield the best results (see Appendix A). Furthermore, this method is not time-consuming and therefore well adapted to the automated

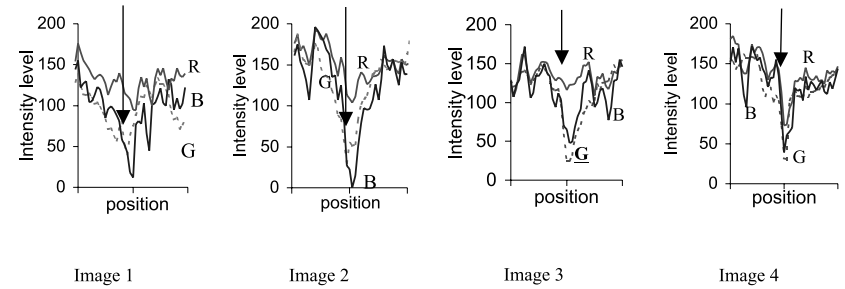

Image 1 Image 2 Image 3 Image 4

(a) Profiles through microcracks

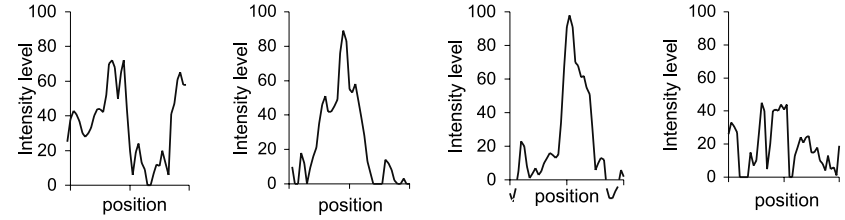

(b) Profiles from combined images (R-G)

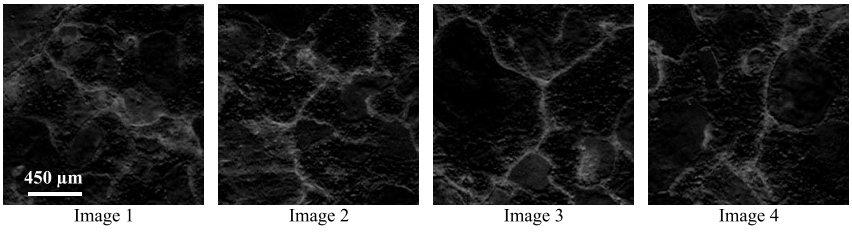

Image 1 Image 2 Image 3 Image 4

(c) Resulted combined images (40X)

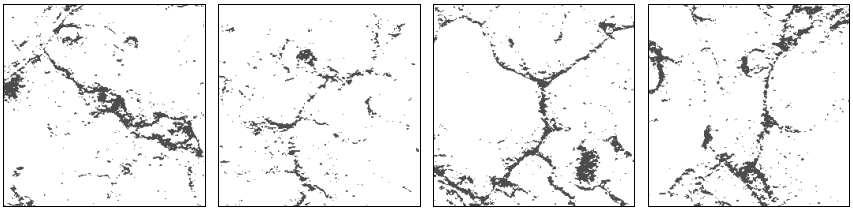

(d) Binary images thresh levels: 52, 66, 51, 50

Fig. 2. Profiles through microcracks and resulting binary images.

treatment of numerous images. Fig. 2(d) shows the resulting binary images.

3.1.2.2. Sample impregnated with fluorescent dye (high performance concrete). For materials impregnated with a fluorescent dye, experience has shown that the contrast of the green component (G) is sufficient and microcracks are well defined on these planes. Fig. 3 shows color images and some statistical parameters corresponding to its components (R, G, B). As can be seen, the range (number of active gray levels) is the widest for the green component (G) which indicates the best contrast. Furthermore, high performance concrete mixtures are less porous than ordinary concrete, so the amount of bright pixels (relatively high gray levels) of the green plane is closely related to the presence of microcracks (Fig. 4). A very simple algorithm was therefore developed for the treatment of these samples. The algorithm consists in maximizing the entropy (see Appendix A) of the green plane [18].

3.1.3. Treatment of the binary images

These initial treatments based on the characteristic gray level of the impregnated defects are not sufficient to extract the microcracks from the image. In fact, the various objects that have been segmented during these operations are not limited to microcracks. They also include various other defects such as air bubbles, various kinds of pores and some porous aggregate particles that have been impregnated during the preparation of the

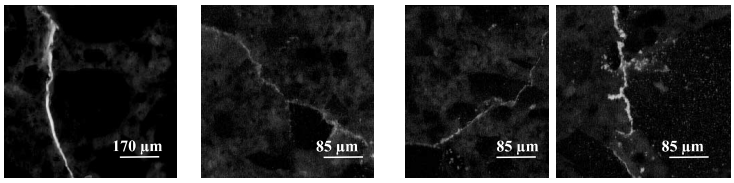

	R	G	B	R	G	B	R	G	B	R	G	B
m	2.4	17.8	12.7	11.7	33.8	10.0	9.0	25.5	9.2	9.6	28.6	11.5
s	14.2	35.1	26.9	15.4	26.0	17.6	13.5	22.7	16.8	17.0	34.1	19.5
range	205	**256**	251	124	**245**	138	110	**256**	165	174	**256**	168

Fig. 3. Color image of high performance concrete.

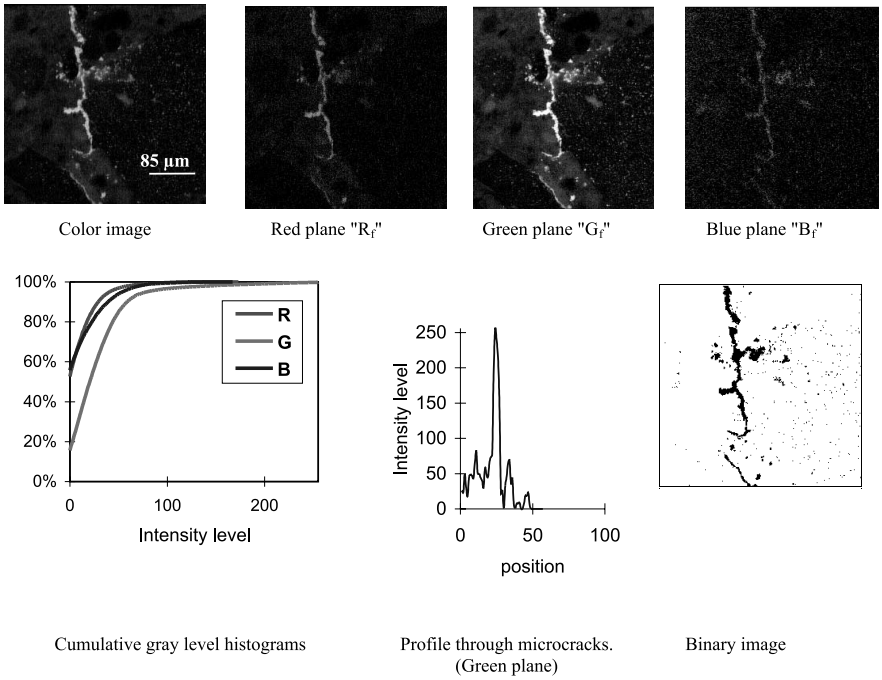

Fig. 4. Color image of high performance concrete and the resulting binary image.

sample. A second series of operations is therefore required to extract the microcracks. A four-step algorithm is used, as summarized below. Figs. 5(a) and (b) present the various steeps of the algorithm:

(1) *Image cleaning*: This operation aims at eliminating from the image small insignificant and isolated particles (f.i. whose width is less than 14.4 μm at magnification 40×) resulting from thresholding operation without affecting the other objects. This objective is achieved by performing an erosion [19] by a structuring element of size 1 (square grid, 8 connexity), followed by a geodesic reconstruction. A morphological closing (dilation + erosion) performed with the same structuring element of size 1 completes the operation.

(2) *Shape analysis*: Experience has shown the need of an additional criterion based on the shape of the objects to eliminate particles that are not microcracks. Cracks can be individual objects with an elongated shape. However, they are in most cases arranged into a connected network. During the development of this method, various shape factors were tested [16,17]. A criterion based on the ratio (F_c) of the true area (A_{ob}) of an object to the area (A_{CC}) of its least circumscribed circle centered on its center of gravity was found to be the most efficient way to distinguish microcracks from other objects. The systematic analysis of standard samples has indicated that 94% of the microcracks are characterized by F_c values which are lower than 0.2. Based on these results, all particles with $F_c < 0.2$ are considered to be microcracks. The validity of this criterion has been verified for the range of magnification used in this study.

(3) *Edge corrections*: The various objects that have been selected on the basis of the previous criterion may be parts of particles that look like microcracks but which are not microcracks. This happens for objects (for instance porous zones) partially masked by the

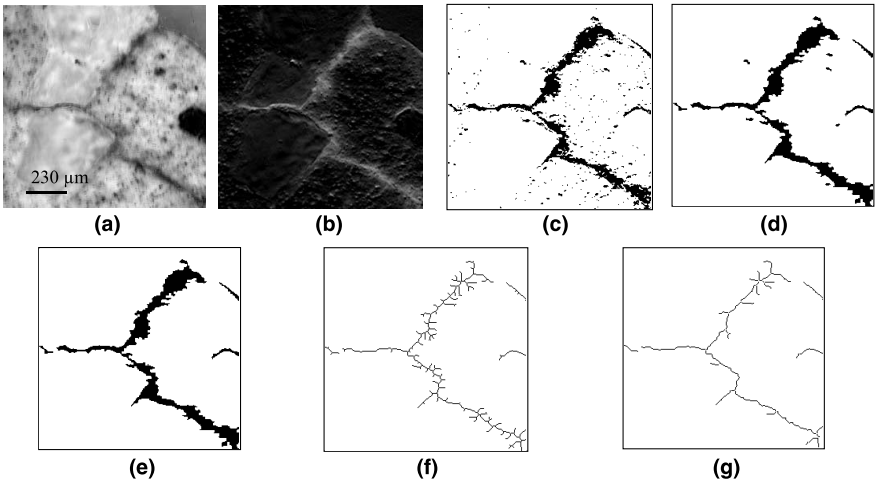

Sample impregnated with red dye

(a) : original color image ; (b) pretreated image, (c) binary image after thresholding ; (d) image cleaning (e) shape analysis ; (f) Skeleton; (g) Skeleton after pruning of size 10

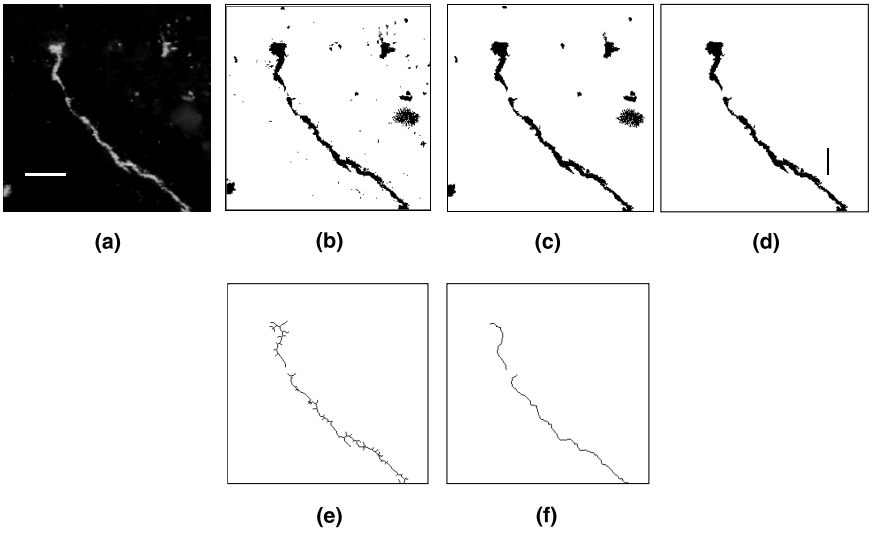

Sample impregnated with fluorescent dye

(a) : original color image ; (b) binary image after thresholding; (c) cleaned image ; (d) image after shape analysis; (e) Skeleton; idealized thin lines ; (f) Skeleton after pruning of size 10

Fig. 5. Major steps of image analysis algorithm.

edges of the images. Hence, an additional criterion has been elaborated in order to automatically discriminate microcracks between subsets of others particles. During the treatment of the image, it is assumed that an object with the azimuth counterclockwise of its greatest projected breadth (Feret's diameter) belonging to $[-10°, +10°]$ when cutting a horizontal edge or belonging to $[80°, 100°]$ when cutting a vertical edge is not a microcrack. This criterion was established and experimentally verified in many cases [16], obviously it must be carefully used when analyzing new unknown materials.

(4) *Skeletonization and pruning of the skeleton*: At the beginning of this step, particles of binary images are assumed to be microcracks. However, the final objective of the operation is to obtain a set of thin lines rather than a set of thick microcracks. Therefore, the skeleton [20] of each binary image is first computed. Then, a skeleton pruning of size 10 is performed in order to clean the extraneous skeleton branches: a pruning of size n consists in removing n pixels of each branch of the skeleton starting from each of its endpoint. At the end of the pruning operation, microcracks are obviously simplified and reduced in length. Nevertheless, it should be

emphasized that the numerous advantages of the method largely compensate for its inconvenience.

At the end of this operation, the set of binary images is now ready for length and orientation measurements.

3.2. Automated measurements

At the end of the previous binary image treatment, microcracks look like curved and branched thin lines. It is therefore possible to estimate their length and their orientation. Since the observation is performed in a two-dimensional space, one needs to compute parameters than can give information about the three-dimensional reality. For this purpose, the characteristics of the microcrack pattern are determined on the basis of methods suitable for the calculation of stereological parameters.

During the development of this image analysis procedure, two different methods were implemented and tested: a first technique of measurement based on the projection method and a second one based on the intersection method [21–23].

Projected breadth measurement or the total projection method: Some multiple points and loops remain after the pruning and cleaning operations. In order to avoid major overlaps when projecting microcracks in a given direction, the first step of this method consists in separating the connected branches of the skeleton. Unfortunately this method cannot eliminate the loops. Then, the projected breadth (D: Feret's diameter) can be measured in any direction $D(\theta)$ assuming that this method of measurement systematically underestimates the projected length of the microcracks. Roses of the projected length density $L_A(\theta)$ can be obtained (Fig. 6(a)). The degree of orientation (ω) can be computed according to the following equation:

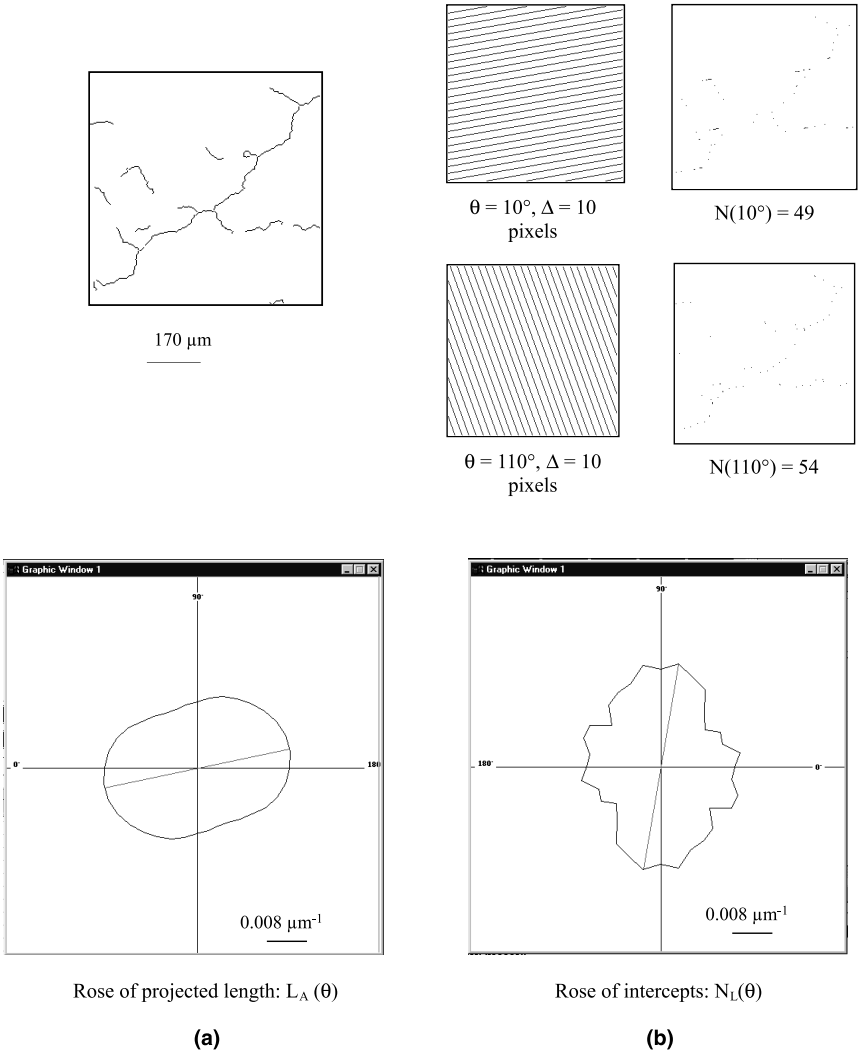

Fig. 6. Example of automated quantification by two methods.

$$\omega = \frac{L_{A\mathrm{or}}}{L_{A\mathrm{tot}}} = \frac{L_{A\mathrm{or}}}{L_{A\mathrm{or}} + L_{A\mathrm{iso}}}, \quad 0 \leqslant \omega \leqslant 1, \tag{2}$$

where $L_{A\mathrm{iso}}$ and $L_{A\mathrm{or}}$ are the isotropic and oriented specific lengths, respectively, and $L_{A\mathrm{tot}}$ is the total specific length of cracks.

Intersection counting measurement or the oriented secant method: Following the method developed by Steinhaus [24] and using an automatic procedure implying logical binary operations of the images, one can proceed as follows: a set of parallel equidistant lines with a given direction is superimposed on an image and the number N of intersections of the microcracks with the set of lines is measured; the number $N(\theta)$ of intersections for a total length of lines L is obtained. By rotating the set of reference lines, one can get another series of $N_L(\theta)$ values. These values can be represented on a polar diagram (Fig. 6(b)). In this study, the influence of several factors on the measurements (spacing between lines, definition of the number of intersections) was evaluated [16]. The degree of orientation can be computed according to the following equation:

$$\omega = \frac{(N_{L\max} - N_{L\min})}{N_{L\max} + \left(\frac{\pi}{2} - 1\right) \cdot N_{L\min}}, \quad 0 \leqslant \omega \leqslant 1, \tag{3}$$

where $N_{L\max}$ and $N_{L\min}$ are the maximum and minimum values taken by $N_L(\theta)$ when θ varies. ω takes the value 0 for a perfectly isotropic crack network (i.e., with no special orientation) and the value 1 when all the microcracks have the same orientation.

In the case of an isotropic crack network, the average number of intersections N_L (which is in this case independent on θ, the total specific length and the specific area of cracks $S_V(\mathrm{mm}^2/\mathrm{mm}^3)$ can be calculated as follows:

$$\frac{\pi}{2} \cdot N_L = \overline{L_A} = \frac{\pi}{4} \cdot S_V. \tag{4}$$

Experience has shown that, when optimized, both methods yield globally the same results: the difference on the density and degree of orientation measurements is less than about 5% and 20%, respectively [16]. However, the method of total projections is less time-consuming (by a factor approximately 3). This method was therefore selected, and implemented in the final algorithm. Obviously, it will be necessary to be careful when applying this method to new materials.

3.3. Reconnecting of microcracks

The various steps of the algorithm previously described enable to obtain local data (for each individual field in a sample). However, cracks can extend on several neighboring microfields. If no particular attention is paid to this particularity, large cracks will be counted as several different smaller cracks.

This does not induce any significant error on the values of N_L or L_A. It can however have a detrimental effect on the prediction of the material physical properties, which are derived from crack pattern estimates. Thus, it appears that the determination of more global parameters, like the crack length distribution, can be very useful. The main difficulties arise from the complex geometry of the cracks (tortuous, branching, ...).

During the course of this work, a specific algorithm was developed to re-connect large cracks [16]. The problem is simplified by considering only the crack ends stored in each field. For each crack (i) contained in a given field, all potential "twin" cracks (j) in the neighboring fields are tested. Two criteria must be fulfilled for connecting crack i to crack j:

1. the distance between two cracks must be lower than $\Delta_{\max}$, which is an error value due to the imperfect translation of the specimen (mechanical gap in the guidance system that can be carefully estimated) and,
2. the angle between the two cracks must be larger than 90° (obtuse). This value has been chosen to account for the phenomenon of branching (see Section 4) and aims to "rebuild" the longest microcracks.

Several tests were performed to validate the various steps of the image analysis procedure. These tests were carried out on both artificial specimens and on real cracked material. Furthermore, sources of errors, reproducibility and accuracy limits of the measurements are widely discussed in [16,17].

3.4. A complementary algorithm for segmentation of macrocracks

The mechanical degradation of granular materials (such as concrete) results in the formation of macrocracks. Macrocracks are known to have a major influence on various macroscopic properties such as permeability [3,25]. The image analysis algorithm must therefore be able to identify and quantify macrocracks properly.

Beyond a certain crack opening, estimated to be about 10–15 μm, the pixels corresponding to large cracks have low gray levels in the images obtained for a sample impregnated with a red dye (Fig. 7). Consequently, cracks cannot be directly segmented using the same approach as that described for microcracks (Section 3.2). A complementary analysis is thus needed to locate and extract these cracks. Experience has shown that the thresholding of the red plane (R) of the color image generally yields reasonable results. However, there are some more complex cases, mainly when a dark particle is connected to the crack. Without correction, this phenomenon tends to overestimate the breadth of the crack. To resolve such

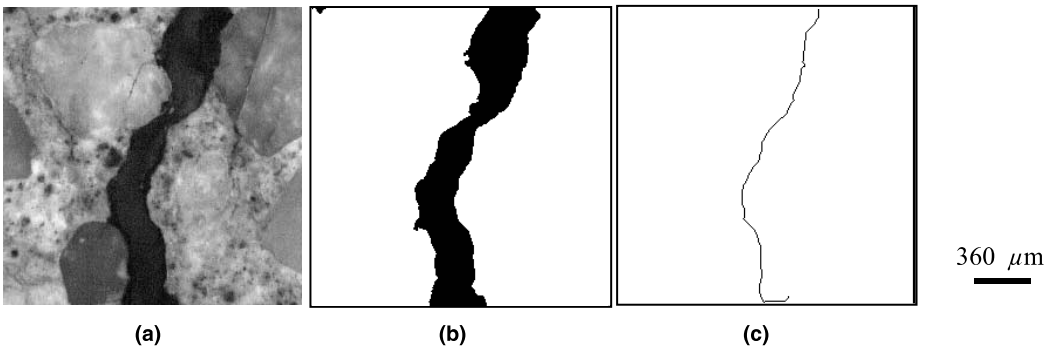

Fig. 7. Example of macrocracks segmentation.

cases, a semiautomatic procedure involving a graphic loop is used to correct the thresholding result: a question is asked during the systematic displacement of the sample about adequacy of segmentation for a current field. The operator can also make correction on an overlay of the color image using a mouse.

Once the cracks are segmented in the image, they are treated using the same procedure as that described previously (Fig. 7). The quantitative characteristics of macrocracks (L_A or $S_v, L_A(\theta)$ et ω) are also determined using the method of the total projections. Furthermore, an evaluation of the apparent crack opening can be made on the basis of the image analysis procedure. Using a simplified approach, the mean width of each crack ($e_{c\,mean}$) is computed as the ratio between the area of the object and the length of its skeleton (Fig. 7(b–c):

$$e_{c\,mean} = \frac{A_{ob}}{L_{skel}}, \tag{5}$$

where A_{ob} is the area object (μm^2) and $L_{skel}(\mu m)$ is the length of skeleton after the pruning step. A skeleton pruning of size 30 is performed to clean the extraneous skeleton branches. Crack widths computed by this simplified approach are in good agreement with those obtained from a set of manual microscopic measurements [16].

4. Study of a mortar subjected to uniaxial compressive loading

The image analysis technique has been applied to mechanically damaged cement-based materials. The crack network characteristics of a mortar, which had been subjected to different levels of uniaxial compressive loading, are presented. Detailed information on the mixture characteristics, the physical properties of the mortar, and the experimental procedures can be found in references [26,27]. During the uniaxial compression test, the rate of the deformation along the perimeter (ε_2) of the 110×220 mm cylinder was controlled. Samples were analyzed at three levels of loading:

- Level 0: unloaded sample ($\varepsilon_2 = 0$),
- Level 1: sample loaded at 95% of peak load ($\varepsilon_2 = 1.15 \times 10^{-3}$),
- Level 2: sample loaded at post-peak load ($\varepsilon_2 = 3.76 \times 10^{-3}$).

Preliminary studies have indicated that the characteristics of the crack network do not vary significantly along the longitudinal axis of the sample [17]. Therefore, the various samples were sawn from the central portion of the cylinder perpendicularly to the direction of loading.

Once the preparation operation was completed, an area of about 28–44 cm^2 was analyzed for each sample at a magnification of 40×. The choice of a magnification level is essentially a compromise between the time of analysis and the degree of sharpness required [16,17,26]. For example, at a magnification of 40×, the time required to analyze an area of 44 cm^2(= 1295 fields) sample is about 5 h.

Table 1 gives the specific crack length (L_A), the degree of orientation (ω) and the percentage of the uncracked area within specimen (A_{uc}). As can be seen, an increase in loading from levels 0–2 contributes to markedly increase the specific microcracks length and the spatial

Table 1
Crack pattern characteristics of a mortar subjected to a compressive loading

Sample	A (cm^2) [number of images]	L_A (mm^2/mm^3)	ω (%)	A_{uc} (%)
Level 0	27.7 [810]	0.23	21	20.0
Level 1	44.3 [1295]	0.32	36	13.8
Level 2	38.3 [1120]	0.50	15	13.5

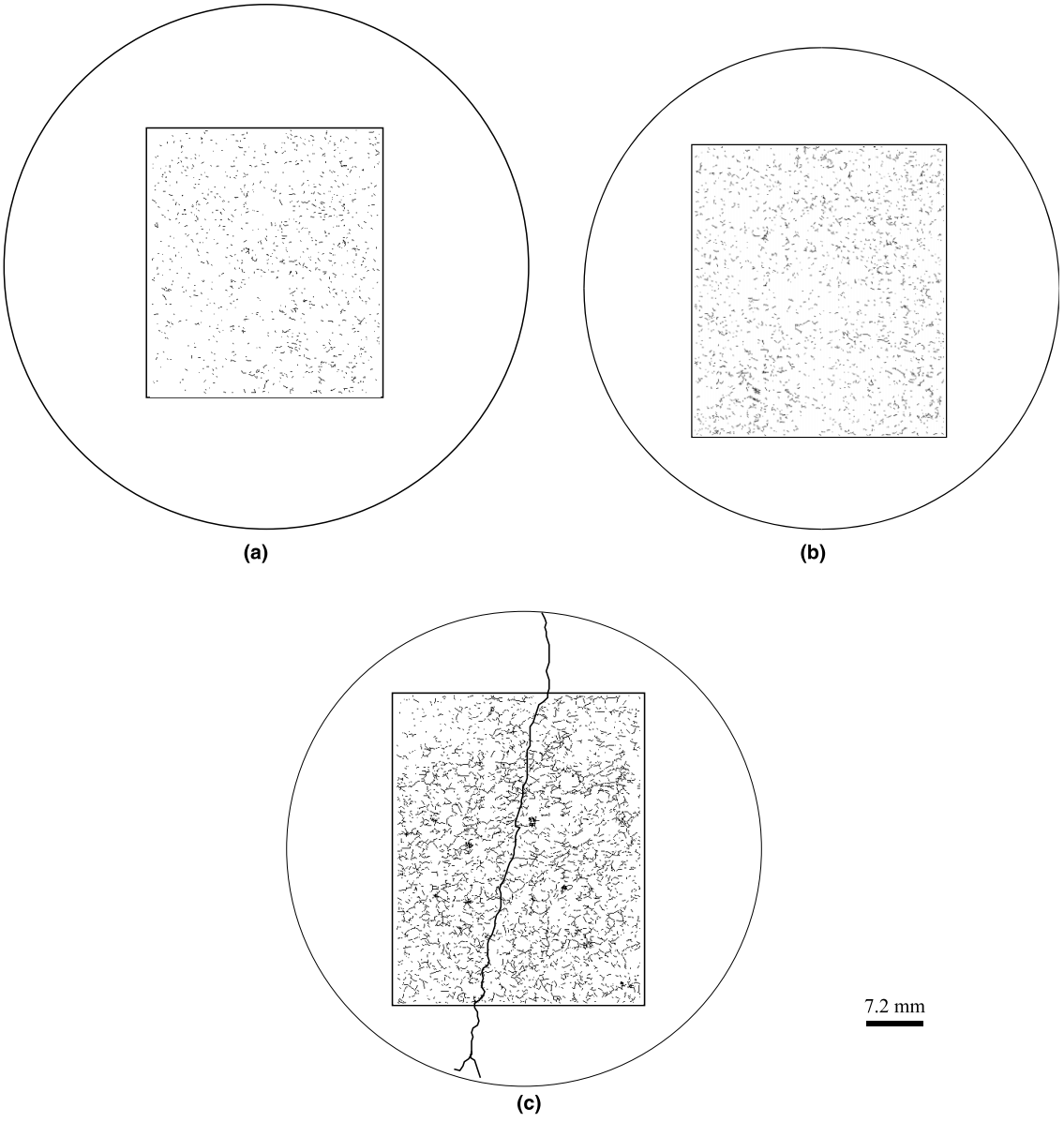

Fig. 8. Cracking pattern of mortar sample: (a) unloaded sample; (b) sample at level 1; (c) sample at level 2.

Fig. 9. Macrocracked area in the mortar sample level 2 (5×2 microscopic field at 40×).

Table 2
Micro and macro cracks measurements for mortar sample of level 2

Parameter	Mortar level 2
Mean macrocrack aperture $e_{c\ macro}$ (μm)	240
L_{micro} (mm)	1915
L_{macro} (mm)	205
L_{macro}/L_{total} (%)	10.6
L_{macro}/ϕ	3.2
ω_{micro} (%)	15.2
ω_{macro} (%)	55.5

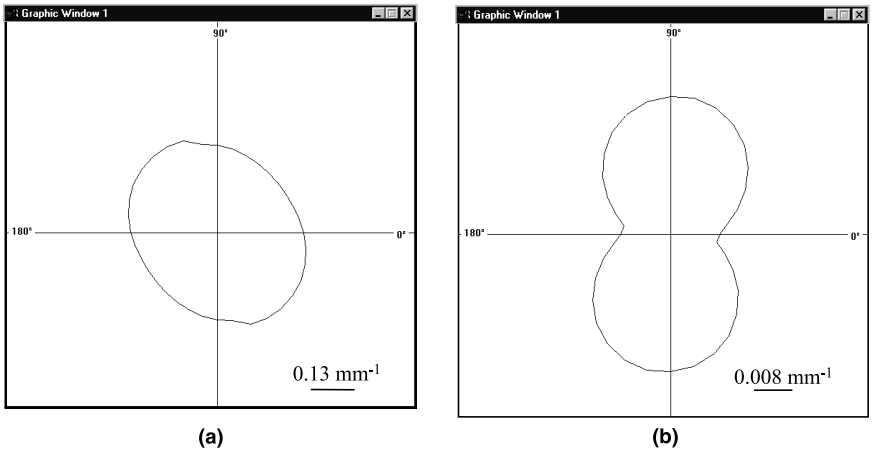

Fig. 10. (a) Rose of specific length of microcracks; (b) rose of specific length of macrocracks.

extension of the damage within material (A_{uc} decreases). The degree of orientation remains low in the plane of observation [26]. Such a phenomenon can be explained by the development of a large number of microcracks around sand particles. These cracks are rather isotropic. Furthermore, Fig. 8 confirms that the crack network appears, at this scale, to be spatially homogenous within the specimen.

A large macrocrack was detected during the preparation of the specimen "level 2". A closer examination revealed rather a complex macrocracked area made of numerous tortuous branches more or less connected to the principal crack in the plane of observation (Fig. 9). As discussed in Section 3.4, such cracks present particular gray levels in the images.

One can quantify these large defects and compare the results with characteristics of the microcracks. An area of 0.9×6.5 cm^2 (5×35 elementary fields) including the principal macrocracks was analyzed at the same magnification factor (40X). Table 2 gives the cracks lengths (L_{macro} and L_{micro}), the degrees of orientation (ω_{macro} and ω_{micro}) and the mean width (e_{macro}) of macrocracks (or apparent aperture). The last value was computed as the mean of width cracks ($e_c > 10$ μm) weighted by theirs lengths. The two ratios: (1) length of macrocracks divided by the total crack length (L_{macro}/L_{total}) and (2) length of macrocracks divided by the specimen diameter (L_{macro}/ϕ) are also presented in Table 2. Figs.10(a) and (b) show, respectively, the roses of specific cracks length for the two categories of defects. The 90° direction corresponds approximately to the orientation of the principal crack.

The following findings are obtained from these observations:

- The macrocrack length represents only about 11% of the total crack length within specimen. However, the macrocracks are significantly more open, and are very likely connected within the volume of the material. The presence of such cracks likely results in a significant increase of the permeability [26].
- The macrocracks present a high degree of orientation, while the microcracks are more isotropic.
- As a consequence of the branching phenomenon previously described in the literature (see, for instance, Ref. [28]), the macrocrack length is greater than the specimen size (110 mm), in this case it is 3.2 times greater.

5. Summary

A technique for the quantification of cracks in cement-based materials has been developed. It includes: (1) an experimental process during which samples are impregnated without inducing any spurious microcracking and (2) a set of image analysis algorithms that enable one to determine the crack pattern characteristics of a given sample and to map the defects. The whole analysis process makes it possible to systematically analyze specimens of significant size with respect to the mechanical representative elementary volume of materials that have been damaged by various mechanisms. The measurements can be qualitatively as well as quantitatively compared for several magnifications.

Acknowledgements

The authors are grateful to Electricité de France (EDF/DER) for its financial support for the project and the GEO Laboratory Network for its cooperation on this topic.

Appendix A. Entropy of a binary image

Let s be a threshold value so the threshold operator maps a gray level image $O_{gl}(x,y)$ into a binary image $O_{bin}(x,y)$: all pixels of the gray level image whose values are greater or equal to s are set to 1 and the other ones to 0.

$$O_{bin}(x,y) = \begin{cases} 1 & \text{if} \quad O_{gl}(x,y) \geqslant s, \\ 0 & \text{if} \quad O_{gl}(x,y) < s. \end{cases}$$

Since the entropy H of a binary image is [29,30]:

$$H[O_{bin}] = -p_s \cdot \ln p_s - (1-p_s) \cdot \ln(1-p_s)$$

(where p_s is the probability of a pixel of the gray level image to have a gray level higher than s) the threshold s is found by computing the maxima of the previous equation.

References

[1] Ziegeldorf D. Phenomenological aspects of the fracture of concrete. In: Wittman FH, editor. Fracture Mechanics of Concrete. Amsterdam: Elsevier, 1983. p. 31–42.

[2] Attiogbe EK, Darwin D. Submicrocracking in cement paste and mortar. ACI Mat J 1987;84:491–500.

[3] Gérard B, Breysse D, Ammouche A, Houdusse O, Didry O. Cracking and permeability of concrete under tension. Mater Struct 1996;29:141–51.

[4] Samaha IB, Hover KC. Influence of microcracking on the mass transport properties of concrete. ACI Mat J 1992;89:416–24.

[5] Slate FO, Olsefski S. X-Rays for study of internal structure and microcracking of concrete. J Amer Conc Inst 1963;60:575–87.

[6] Najjar WS, Aderhold HC, Hover KC. The application of neutron radiography to study of microcracking in concrete. Cem Concr Agg 1986;8:103–109,.

[7] Slate FO. Microscopic observations of cracks in concrete, with emphasis on techniques developed and used at Cornell University. In: Wittman FH, editor. Fracture Mechanics of Concrete. Amsterdam: Elsevier, 1983. p. 75–83.

[8] Ollivier JP. A non destructive procedure to observe the microcracks of concrete by scanning electron microscopy. Cem Concr Res 1985;15:1055–60.

[9] Ringot E, Ollivier JP, Maso JC. Characterisation of initial state of concrete with regard to microcracking. Cem Concr Res 1987;17:411–9.

[10] Hornain H, Moranville-Regourd M. Microcracking of concrete. In: Proceedings Eighth International Congress on the Chemistry of Cement. Rio de Janeiro, 1986. V: p. 5359.

[11] Hornain H, Marchand J, Ammouche A, Commène JP, Moranville M. Microscopic observation of cracks in concrete A new sample preparation technique using dye impregnation. Cem Concr Res 1996;26:573–83.

[12] Darwin D, Ketcham KW, Romero FA, Martin JL. Automated identification of compression induced cracking in cement paste. In: Proceedings ASCE Eng. Mech. Conf. College station, Texas, 1992. p. 494–497.

[13] Moranville-Regourd M. La durabilité des structures en bétons. Conf. Paris: LNPC, France, 1990.

[14] Darwin D, AbouZeid MN, Ketcham KW. Automated crack identification for cement paste. Cem Concr Res 1995;25:605–16.

[15] Gran HChr. Fluorescent liquid replacement technique. A mean of crack detection and water binder ratio determination in high strength concrete. Cem Concr Res 1995;25:1063–74.

[16] Ammouche A. Caractérisation automatique de la micro fissuration des bétons par traitement d'images. Application à l'étude de différents faciès de dégradation. Ph.D. thesis. Bordeaux-Québec, Laval Université Bordeaux 1 (France)/Université Laval (Canada), 1999.

[17] Ammouche A, Breysse D, Hornain H, Didry O, Marchand J. A new image analysis technique for the quantitative assessment of microcracks in cementbased materials. Cem Concr Res 2000;30:25–35.

[18] Van der Heijden F. Image based measurement systems, object recognition and parameter estimation. Chichester: Wiley, 1994.

[19] Chermant JL. Why automatic image analysis. This proceedings.

[20] Soille S. Morphological Image analysis. Principles and applications. Berlin: Springer; 1999.

[21] Saltykov SA. Stereology. In: Helias H, editor. NewYork: Springer, 1967.

[22] Underwood EE. Quantitative stereology, Reading Massachusetts, Series in Metallurgy and Materials. Addison-Wesley, New York, 1970. p. 23–47.

[23] Stroeven P. Some aspects of the micromechanics in concrete, Ph.D. thesis. Delft: Delft University, 1973.

[24] Santalo LA. Integral geometry and geometric probability. London: Addison-Wesley; 1976.

[25] Wang K, Jansen DC, Shah SP. Permeability study of cracked concrete. Cem Concr Res 1997;27(3):381–93.

[26] GEO. La dégradation des bétons. Couplage fissurationdégradation chimique, In: Torrenti JM, editor. Hermes Science Publications, 1999. p. 7587.

[27] Tognazzi C. Couplage fissurationdégradation chimique dans les matériaux cimentaires: caractérisation et modélisation. Thèse de doctoral INSA. Toulouse, Université de Toulouse, 1998.

[28] Diamond S, Mindess S. Scanning Electron Microscopic Observations of Cracking in Portland Cement Paste. Proceedings Seventh International Congress on the Chemistry of Cement. Paris: 1980. III p. VI-114–VI-119.

[29] Kapur JN, Sahoo DK, Wong AKC. A new method for grey-level picture thresholding using the entropy of the histogram. Computer Vision Graphics and Image Processing 1985;29:273–85.

[30] Pinoli JC. Contribution à la modélisation, au traitement et à l'analyse d'image. Thèse. Saint Etienne, Université de Saint Etienne, 1987.